Surface structural characteristics and tunable electronic properties of wet-chemically prepared Pd nanoparticles

S. C. Cook, J. D. Padmos, and P. Zhang

Citation: The Journal of Chemical Physics **128**, 154705 (2008); doi: 10.1063/1.2901034
View online: http://dx.doi.org/10.1063/1.2901034
View Table of Contents: http://scitation.aip.org/content/aip/journal/jcp/128/15?ver=pdfcov
Published by the AIP Publishing

Surface structural characteristics and tunable electronic properties of wet-chemically prepared Pd nanoparticles

S. C. Cook, J. D. Padmos, and P. Zhang[a)]
Department of Chemistry and Institute for Research in Materials, Dalhousie University, Halifax, Nova Scotia B3H 4J3, Canada

(Received 25 January 2008; accepted 27 February 2008; published online 16 April 2008)

The ligand substitution reaction, Pd $L_{3,2,1}$-edge and S *K*-edge x-ray absorption fine structure (XAFS), XAFS simulations, and valence-band and core-level x-ray photoelectron spectroscopy (XPS) have been used to systematically study the surface chemical and electronic properties of wet-chemically prepared Pd nanoparticles of varied size, molecular capping, and metal composition. It was found that the replacement of weakly interacting capping molecules (amine and tetra-alkylphosphonium bromide) with strongly binding thiols caused a considerable change in the surface bonding of Pd nanoparticles. However, the Pd *d*-electron counts (number of *d* electrons) remained almost unchanged before and after ligand substitution, which is unexpected since Pd atoms normally lose electrons to the more electronegative S atoms. XAFS results and simulations provided useful insights into the surface structural characteristics of Pd nanoparticles and satisfactorily accounted for the unexpected *d*-electron behavior involved in the ligand substitution process. XPS valence and core-level spectra further revealed a size-dependent *d*-band narrowing and presented complementary information to XAFS about the surface electronic properties of Pd atoms. The small weakly bound Pd nanoparticles seem inevitably to have a net *d*-electron depletion due to the influence of the surface effect (chemical adsorption by oxygen), which is more significant than the *d*-electron enriching nanosize effect. However, it was demonstrated that by forming Pd–Ag alloy nanoparticles, a net increase of the Pd *d*-electron counts can be realized. Therefore, it is illustrated that by manipulating the surface, size, and alloying effects, the electronic properties of Pd nanoparticles can be possibly tuned. © *2008 American Institute of Physics*.
[DOI: 10.1063/1.2901034]

I. INTRODUCTION

Studies on the structural and electronic properties of metal nanoparticles have stimulated intense research interest over the past three decades.[1–10] A key issue is the elucidation of the structure-property relationships of metal nanoparticles, which are of paramount importance in both fundamental studies and technological applications, such as catalysis.[1,9–12] Traditionally, metal nanoparticles have been prepared on solid substrates and are denoted as substrate-supported nanoparticles (SNPs) in this paper. The preparation of SNPs is usually based on vacuum evaporation methods, requiring the use of large instruments.[1–5] Recently, significant advances have been achieved in the wet-chemical synthesis of molecularly capped nanoparticles (MNPs) of metals.[13–19] From the viewpoint of sample preparation, the wet-chemical method shows various advantages over the vacuum evaporation one, such as low preparation cost and better control of nanoparticle structure with regard to size, monodispersity, and shape.[13–19] From the perspective of the crystalline structure and electronic properties of metals, a MNP can be approximately considered as an analog to a SNP in that both of them consist of nanosized crystal fragments, thus showing many common electronic properties, such as incomplete band structure[2] and quantum confinement of electrons.[14] However, the most striking difference between them is that the surfaces of MNPs are capped with organic molecules. The capping molecules (in some references also called ligands) serve to surface functionalize as well as stabilize the nanoparticles. Many promising applications can be foreseen in association with the molecular capping of MNPs in areas such as biodetection,[20] drug delivery,[21] and chiral catalysis.[22] In this context, it is very important to understand the surface chemical and physical properties of the MNPs in connection with the wet-chemical synthesis and metal-ligand interaction.

Although the structural and electronic properties of metal SNPs have been well documented (this has been particularly successful based on x-ray spectroscopic studies[1–6]), a detailed picture of the surface chemical and physical properties of metal MNPs, particularly from the electronic perspective, is still lacking. To contribute to this, we will present results from a thiol substitution reaction of capping molecules, the Pd $L_{3,2,1}$-edge and S *K*-edge x-ray absorption fine structure (XAFS), XAFS simulations, and valence and core-level x-ray photoelectron spectroscopy (XPS) of Pd MNPs with varied size, surface capping, and metal composition. The purpose of this work is threefold. First, it is intended to use the well developed framework of the surface science of two dimensional (2D) metals and SNPs to understand the properties of MNPs. Specifically, complementary x-ray spec-

a)Author to whom correspondence should be addressed. Electronic mail: peng.zhang@dal.ca.

troscopic techniques such as XPS and XAFS, which have been highly successful in the studies of 2D metals and SNPs, are employed in the present work. Second, we intend to explore the structural and electronic properties of MNPs that are associated with the wet-chemical synthesis and molecular capping, which is absent in their SNP counterparts. In this case, a ligand substitution reaction was conducted to replace the original weakly binding molecules with strongly binding thiols, so that the properties of MNPs of the same size but with different capping molecules could be comparatively studied. Finally, this study seeks to find an efficient way to tune the electronic properties of transition metal MNPs. Specifically, it is intended to control the *d*-electron counts of Pd atoms in the nanoparticles. This is of great importance in designing nanoparticle catalysts with controllable reactivity and/or selectivity.[1,23,24] We have shown that the size and capping effects can be utilized to some extent to tune the *d*-electron counts (i.e., the average number of *d* electrons per atom) of Au MNPs.[25,26] In this contribution, we extend our work to the study of Pd, a very important metal in catalysis, and demonstrate that the tunable *d*-electron behavior of Pd can be achieved by manipulating the size, surface, and alloying effects.

II. EXPERIMENTAL SECTION

A. Synthesis and characterization of nanoparticles

The metal MNPs were prepared by reducing palladium acetate compounds (with silver acetate in the case of the Pd–Ag sample) in toluene in the presence of 80% dodecyl amine (DDA) and 20% didodecyldimethyl ammonium bromide (DDAB) or tetraoctylphosphonium bromide surfactants (TOPB). The use of DDA/DDAB led to Pd MNPs of 4.5 nm; using DDA/TOPB produced 2.7 nm MNPs. The molar ratio of metal compound to capping molecules in the starting materials was kept at 1:15. Using a combination of two types of capping molecules (amine and bromide surfactants) can ensure that the MNPs are stable enough to be purified and are fairly monodispersed. In this regard, DDA serves to enhance the stability of the MNPs so that the MNPs can be purified by centrifuge and the purified products are redispersible in nonpolar solvents. We found that if only DDAB or TOPB were used as capping molecules, the products were unstable and difficult to purify. On the other hand, relative to the strongly binding thiols, DDAs are still considered as weakly binding molecules as they can be easily replaced in the subsequent thiol substitution reaction. For such a reason, all the nonthiol-capped samples are called weakly bound MNPs in the following discussions. The purpose of using DDAB and TOPB is to achieve good monodispersity of the MNPs.[27] In addition, different bromide surfactants, i.e., DDAB and TOPB, are used to control the nanoparticle size, similar to the preparation of Au MNPs.[27] The synthetic procedure for Pd MNPs is as follows. The metal compound and capping molecules were first dissolved in toluene by sonication. Under Ar bubbling and stirring, ten times (molar ratio) of sodium borohydride (with 20 μl water) was added to reduce the metal compounds into metallic MNPs, and the reactions were further kept running for 2 h under Ar protection. Most of the toluene was then removed by a rotary evaporator. Next, 100–200 ml ethanol was added to the reaction mixture to cause precipitation. The precipitate was collected by centrifuge and was redispersed with toluene and centrifuged again to remove the insoluble components. Finally, the purified samples were stored in toluene under Ar protection. The purified MNPs were stable for more than three months without a visible precipitate. The ligand substitution reaction was conducted by adding dodecanethiol to the DDA/TOPB capped 2.7 nm Pd MNPs (molar ratio of Pd:S=1:10) under Ar protection, and the mixture was kept stirring for 1 h. After that, centrifuge purification was performed to obtain purified products.

The morphology of the MNPs was characterized with a Technai 12 transmission electron microscopy (TEM) equipped with a charge coupled device camera and operated at a voltage of 80 keV. One or two drops of the MNP solution were cast to carbon or formvar-coated Cu grids for the TEM measurements. The particle sizes were obtained by counting more than 200 particles using a size-measuring program from the TEM.

B. XAFS measurements

The XAFS measurements were conducted at the Canadian Synchrotron Radiation Facility (CSRF) DCM beamline at Synchrotron Radiation Center (SRC), University of Wisconsin-Madison. The SRC synchrotron facility was operated at either 800 MeV (for the S *K*-edge XAFS) or 1 GeV (for the Pd $L_{3,2,1}$-edge XAFS) with a beam current of ~250 mA at injection. The x-ray absorption was monitored with a total electron yield (TEY). Although x-ray fluorescence yield (FLY) spectra were also collected, TEY measurements are highly preferred, particularly for the white line (the most intense peak at the threshold) analysis of x-ray absorption near edge structure (XANES) at the Pd $L_{3,2}$-edge.[23] The approach of measuring TEY avoids experimental artifacts caused by sample thickness effects, which is common in the FLY of concentrated samples.[23] The XAFS data were normalized and analyzed using the standard methods previously described.[25,26,28]

C. XAFS simulations

The XAFS simulations were conducted using the *ab initio* self-consistent field code FEFF8.2.[29] A cluster model was first built with a CRYSTALMAKER or CHEM 3D program. Coordinates of the cluster were then used in the FEFF input file. Both site-specific and average spectra[30] were obtained in the simulations. The FEFF simulations of Pd_{55} model clusters adsorbed with sulfur atoms and thiolate groups ($-SCH_3$) were both tested, and the results were found to be essentially the same. Therefore, only simulation results from sulfur-atom-adsorbed models are used in the discussions.

D. XPS measurements

The XPS measurements were carried out with a VG Microtech MultiLab ESCA 2000 System using a Mg $K\alpha$ x-ray source. The MNP samples from solution were cast onto an Al sample holder for the XPS measurement. An Al holder was

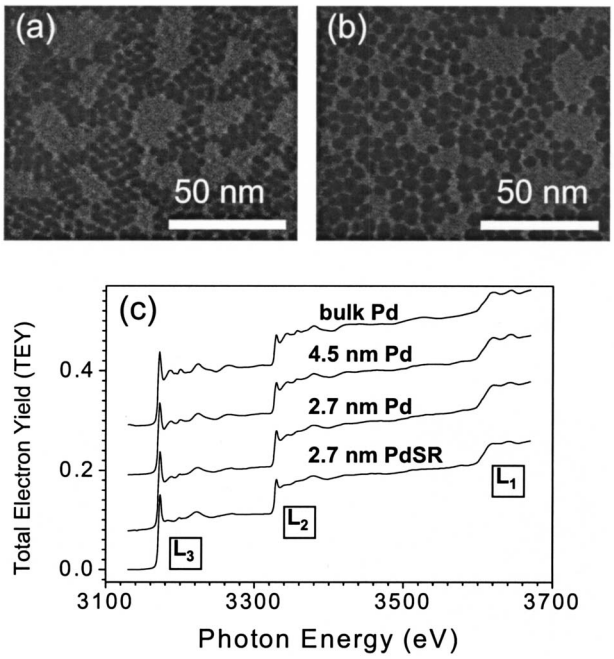

FIG. 1. (a) TEM of DDA/TOPB-capped Pd MNPs. (b) TEM of DDA/DDAB-capped Pd MNPs. (c) XAFS raw data of the three Pd MNPs and bulk Pd at the Pd $L_{3,2,1}$-edges.

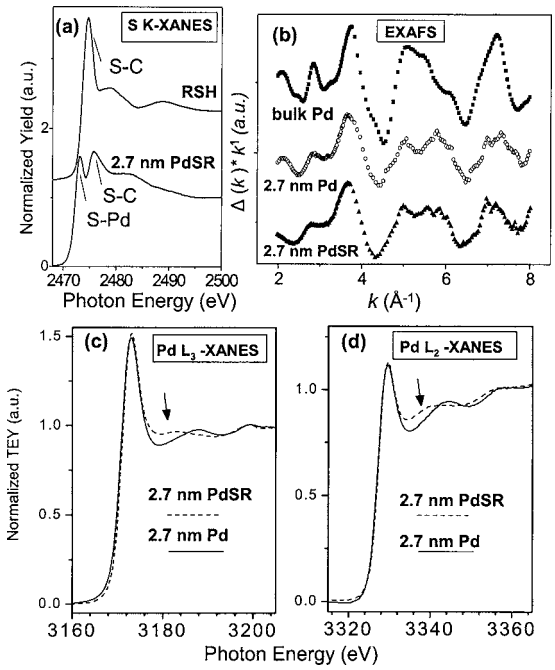

FIG. 2. (a) The S *K*-edge XANES of 2.7 nm PdSR and a free thiol reference. (b) The Pd L_2-edge EXAFS of 2.7 nm Pd, 2.7 nm PdSR, and bulk Pd. (c) The Pd L_3-edge XANES and (d) the Pd L_2-edge XANES of 2.7 nm Pd and 2.7 nm PdSR.

used in order to avoid the charging problem. Meanwhile, due to the surface molecular capping, metal cores of the MNPs should not directly contact the Al substrate. In addition, a Cu sample holder was also used to collect the core-level spectra. The XPS results are essentially the same as those obtained using the Al holder, which further proves that possible contributions from the metal sample holder can be ruled out. To ensure a reliable measurement of the XPS binding energies for all the NP samples, the experiments were performed by mounting all the NPs onto one large Al sample holder consisting of a few small cells, each of which contains one Pd sample. In addition, the Al 2*p* core-level peak was also used to check the accuracy of the measurements of XPS binding energies. The reliability of the binding energy measurements is also verified by the fact that the Pd core-level binding energy data collected from an Al and a Cu sample holder are identical within the experimental uncertainty. Because aluminum does not have a *d* band and will not contribute to the Pd valence-band spectra, only XPS data collected using an Al holder are presented in the discussion.

III. RESULTS AND DISCUSSION

Figures 1(a) and 1(b) show TEM micrographs of the two weakly bound Pd MNPs capped with DDA/TOPB and DDA/DDAB, respectively. By counting more than 200 particles, it was found that the former has an average size of 2.7 nm and the latter has 4.5 nm. From Figs. 1(a) and 1(b), it is evident that both samples are fairly monodisperse. The standard size deviation of the 2.7 nm sample is 17% and that of the 4.5 nm sample is 15%. Moreover, these samples can be purified into powder and redispersed in nonpolar solvent repeatedly. This allows for the collection of high quality XAFS data at the Pd L_3-, L_2-, and L_1-edges; the spectra are shown in Fig. 1(c). The raw data for bulk Pd and 2.7 nm thiol-capped MNPs (prepared by replacing the DDA/TOPB with dodecanethiols) are also shown in the figure. To distinguish the two weakly bound samples from the thiol-capped one, the two nonthiol-capped MNPs are referred to as 2.7 nm Pd and 4.5 nm Pd, whereas the thiol-capped MNPs are denoted as 2.7 nm PdSR throughout this paper. We have also prepared Pd nanoparticles capped with TOPB or DDAB without using DDA. However, the low stability of the samples does not allow us to obtain purified nanoparticles. Consequently, high quality XAFS data could not be obtained and are thus not presented in this paper.

A. XAFS studies of the surface capping effect

To study the surface chemical properties of Pd MNPs, a comparison of 2.7 nm Pd and 2.7 nm PdSR was first made. Figure 2(a) shows the S *K*-edge XANES of 2.7 nm PdSR and a free thiol reference (RSH). The striking difference of the two spectra in Fig. 2(a) immediately shows that after the ligand substitution reaction was performed, thiols bind strongly to the Pd surface. The sharp peak in the spectrum of RSH following the edge jump can be ascribed to the resonance of the S–C bond.[31,32] After thiols bind to the Pd surface, this peak is shifted toward higher binding energies, and its intensity decreases significantly. Meanwhile, a new peak associated with the Pd–S bond appears in the lower binding energy region. Similar spectral features have been reported in the S *K*-XANES of thiol-capped Au MNPs.[26] In addition, a Pd:S molar ratio of 4:1 (uncertainty of 15%) for 2.7 nm PdSR was also obtained by analyzing the area of Pd and S core-level peaks in the XPS. Detailed discussion of the XPS results will be presented later.

The Pd L_2-edge k-space extended XAFS (EXAFS) of the two 2.7 nm samples and bulk Pd are shown in Fig. 2(b). Although quantitative information, such as bond distance and average coordination number, cannot be obtained from the EXAFS near the Pd L_2-edge,[33] a qualitative analysis can still be useful in identifying the structural characteristics of the samples. All the three samples exhibit identical EXAFS oscillating patterns, indicating that all the samples have fcc crystalline structures. The EXAFS oscillations of the bulk, particularly in the high k region, are considerably more intense than those of the two MNPs, whose intensities are essentially the same. The EXAFS oscillation intensity is determined by the average coordination number of Pd atoms in the MNPs.[26] The average coordination number of Pd atoms in the MNPs is considerably lower than that of the bulk. As a result, the MNPs exhibit less intense EXAFS oscillations. The same EXAFS intensity of the two 2.7 nm samples verifies that the ligand substitution does not cause a noticeable change in the particle size. However, considerable differences between these two 2.7 nm samples are found in the Pd $L_{3,2}$-edge XANES shown in Figs. 2(c) and 2(d). The resonance bands (marked by arrows) next to the white lines (the sharp peak right after the edge jump) at both L_3- and L_2-edges shift considerably toward lower binding energies after thiols replace the weakly binding molecules. Such a shift is a signature of the formation of Pd–S bonds on a Pd surface.[31] The Pd $L_{3,2}$-edge white lines are associated with the electronic transitions from the $2p$ state to an unoccupied $4d$ state.[34] The white line intensity is determined by the partial unfilled density of states (DOS) of the Pd $4d$ state. A more intense white line corresponds to higher unoccupied d-DOS (also called d-hole).[35] It can be seen from Figs. 2(c) and 2(d) that binding of thiols to Pd causes an almost unidentifiable change (a very small increase) in the intensity of the Pd $L_{3,2}$-edge white line. A semiquantitative calculation[28] shows that the difference of the average d-hole counts (10-counts of d electrons) between the two MNPs is only $0.02e^-$. Previous Au $L_{3,2}$-edge XANES studies have shown that in thiol-capped Au nanoparticles, Au exhibits a $0.05e^-$ d-electron depletion due to charge transfer to the more electronegative S.[25] Pd has an even lower electronegativity than Au and should thus lose more d electron to S than Au does. In order to discover the origin of such a discrepancy, it is necessary to understand the surface properties of 2.7 nm Pd before the ligand substitution reaction was performed. Therefore, we next turn to the XAFS of weakly bound Pd MNPs of different sizes.

B. XAFS studies of the size effect

In Figs. 3(a)–3(c), k-space EXAFSs near L_2-edge and $L_{3,2}$-edge XANESs of 2.7 nm Pd, 4.5 nm Pd, and bulk Pd are shown. The identical EXAFS oscillation patterns of the three Pd samples in Fig. 3(a) indicate that they all have fcc crystalline structures. Size-dependent changes of the EXAFS intensity are particularly evident in the k-range of 5.5–8.0 $Å^{-1}$, consistent with the TEM results in Figs. 1(a) and 1(b). The most striking feature in the XANES in Figs. 3(b) and 3(c) is that both the L_3 and L_2 white lines of 2.7 nm Pd are considerably more intense than those of 4.5 nm Pd, whose intensities are identical to those of bulk Pd. The more intense white lines of 2.7 nm Pd correspond to higher unoccupied d-DOS or a depletion of d electrons. Using the established method,[28] we semiquantitatively calculate the average d-hole counts in the three Pd samples, and the results are given in Table I. The 2.7 nm Pd is found to show a $0.16e^-$ d-charge depletion relative to the other two Pd samples. In addition, the $L_{3,2}$-edge position of 2.7 nm MNPs is shifted toward higher binding energies by 0.6–0.7 eV relative to 4.5 nm Pd and bulk Pd, whose edges are at the same positions. The edge shifts of the MNPs will be discussed later in association with the XPS data.

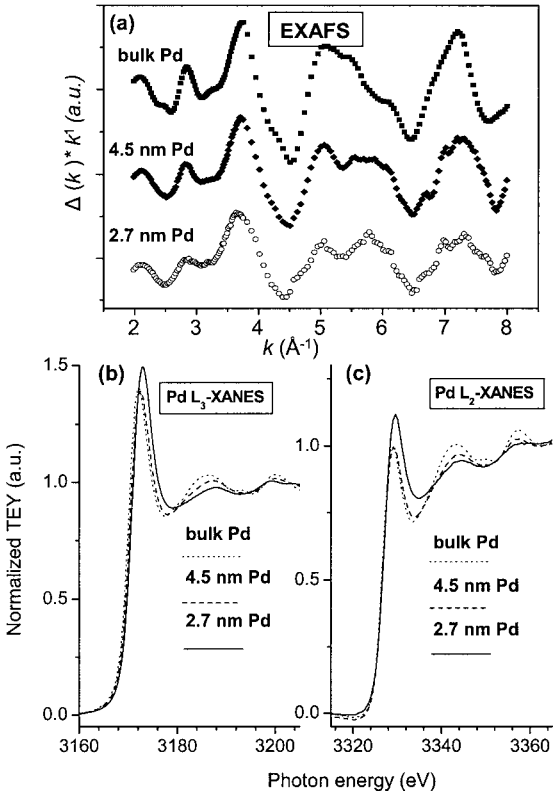

FIG. 3. (a) The Pd L_2-edge EXAFS, (b) the Pd L_3-edge, and (c) L_2-edge XANES of 4.5 nm Pd, 2.7 nm Pd, and bulk Pd.

It has been reported that in weakly bound small Au nanoparticles, the net d-electron counts increase as the size decreases.[25,36] This disagrees with the results for 2.7 nm Pd observed in Fig. 3. An increase of d-electron counts (relative to the bulk) when the coordination number is decreased in metals with nearly full d orbitals has been widely accepted.[4,5,25,36–38] In the studies of metal SNPs, Citrin and Wertheim[4] and Wertheim *et al.*[5] proposed a simple model to interpret this phenomenon by considering the electronic configuration of a single metal atom and the bulk. For instance, the Au and Pd single atoms have completely filled d orbitals, with electronic configurations of $5d^{10}6s^1$ and $4d^{10}5s^0$, respectively. In the bulk, the d band is formed and due to s-p-d rehybridization, the valence d band becomes partially unfilled.[2] Theoretical calculations suggest that bulk Au and Pd should have electronic configurations of $5d^{9.6}$ and $4d^{8.2}$, respectively.[25,28] Thus, when going from the bulk to the

TABLE I. White line parameters of Pd nanoparticles and bulk.

Sample		ΔE_0[a]	White line intensity A[b]	White line intensity ΔA $(A-A_{\text{bulk}})$	d-hole[c] h_t	d-hole[c] Δh_t
Bulk Pd	L_2	⋯	8.8	⋯		
	L_3	⋯	12.1	⋯	1.78	⋯
4.5 nm Pd	L_2	0	9.0	0.2		
	L_3	0	12.1	0	1.78	0
2.7 nm Pd	L_2	0.6	10.3	1.5		
	L_3	0.7	13.0	0.9	1.94	0.16
2.7 nm PdSR	L_2	0.9	10.5	1.7		
	L_3	1.1	13.1	1.0	1.96	0.18

[a]Shift of E_0 of the MNPs relative to bulk Pd. The uncertainty is ±0.3 eV for L_3 and ±0.5 eV for L_2.
[b]Integration of area by taking −10–10 eV near the L_3-edge.
[c]Calculation using Ag L_3-edge and Pd L_3-edge XANESs. The d-hole counts of Ag (0.856) and Pd (1.784) are taken from the literature (Ref. 28). The uncertainty is about 10%.

single atom, the d-electron counts increase. In metal nanoparticles, the valence d band is narrower as the size decreases.[38] As a result, the s-p-d rehybridization is less pronounced than in the bulk (i.e., less overlap of the d band with the s-p band). Therefore, the d-electron counts of metal nanoparticles increase as the size decreases. It should be noted that Wertheim's model is only valid when the surface effects of the nanoparticles are too weak to be considered. This is generally true for a metal surface bound with weakly interacting molecules (e.g., DDA, TOPB, and DDAB), as the interaction is too weak to influence the electronic properties of metals.[39] However, due to the wet-chemical nature of the MNP synthesis, surface effects should not be limited to the interaction between Pd and capping molecules. In order to consider other surface effects that might originate from the wet-chemical synthesis, we next turn to the results of Pd L_1-edge XANES. Pd K-edge XANES, the mechanism of which is very similar to that of L_1-edge XANES, has been recently used as a useful tool to detect oxygen adsorption on Pd nanoparticle surfaces.[40,41]

In the Pd L_1-edge XANES in Fig. 4, three fine structures (labeled a, b, and c), which are characteristic of metallic Pd, are found within 50 eV above the edge in all the three samples. Two interesting observations are noted by comparing these fine structures among the three samples. First, peak b of 2.7 nm Pd exhibits an unusually high intensity on the higher binding energy side (marked by an arrow) relative to the other two samples. Second, peak c of the two MNPs shows a size-dependent shift toward lower binding energies relative to the bulk. The 2.7 nm sample exhibits the largest shift (~2 eV) toward lower binding energies. The first observation is very similar to the Pd K-edge XANES result for partially oxidized Pd nanoparticles recently reported.[40,41] Pd L_1-edge XANES originates from a $2s$ to $4p$ transition, whereas the K-edge spectrum originates from $1s$ to $4p$. A similar origin of the electronic transitions results in very comparable XANES features above the two edges. In a series of *in situ* Pd K-edge XANES studies, it has been reported that when the Pd surface undergoes oxidation with increasing amounts of O_2, the peak maximum of b and the higher binding-energy side of the peak gradually become more intense, whereas peak c becomes less intense. The fact that 2.7 nm Pd does not show considerable change in the intensity of peak b maximum, but only a noticeable increase in the intensity at the higher binding-energy side, implies a slight oxidation of the Pd surface (only a small fraction of surface Pd atoms have adsorbed O atoms). This agrees with the Pd EXAFS results in Fig. 3(a), showing that most of the atoms in the MNPs are still metallic Pd. It is also consistent with the fact that the MNP synthesis was carried out under Ar protection, thus ruling out the possibility of severe oxidation by O_2. However, due to the wet-chemical nature of the synthesis, O atoms from other sources can still be possibly adsorbed onto the Pd surface. In the second observation, peak c shifts toward lower binding energies as the MNP size decreases, leaving a smaller gap between peaks b and c. This coincides with the Pd L_1-XANES result of Pd SNPs reported by De Crescenzi *et al.*, who ascribed the shift of peak c to an increased Pd–Pd bond distance.[42] A series of theoretical and experimental studies have pointed out that in free Pd nanoparticles, there should be a lattice contraction.[43–45] The lattice contraction in metal nanoparticles can be easily understood using a simple liquid drop model; that is, the particle

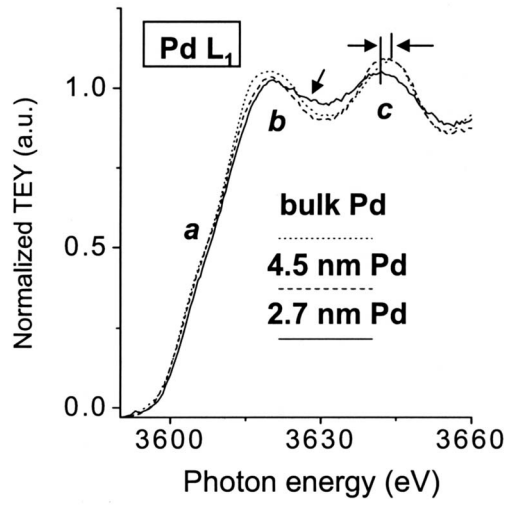

FIG. 4. The Pd L_1-edge XANES of 4.5 nm Pd, 2.7 nm Pd, and bulk Pd.

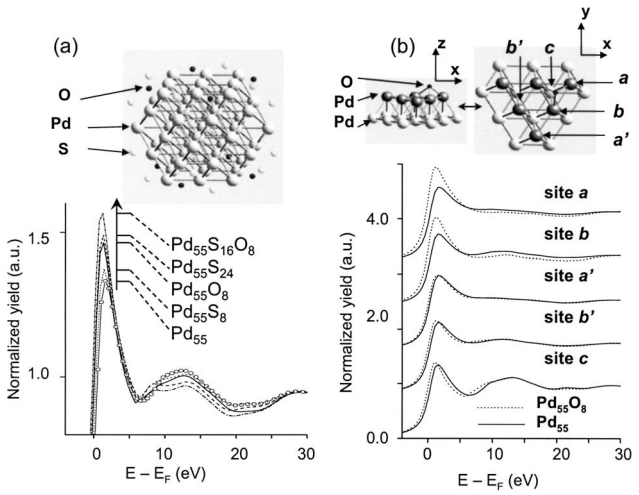

FIG. 5. (a) Average spectra and (b) site-specific spectra of FEFF8 simulated Pd L_3-edge XANES of various Pd cluster models. The model schematically shown in (a) is a $Pd_{55}S_{16}O_8$ cluster and in (b) is part of the $Pd_{55}O_8$ cluster viewed from y and z directions, respectively. The white line maximum positions of the average spectra of different clusters are also marked in (a) with short bars perpendicular to the arrow near the white lines.

surface tends to shrink to decrease the high surface energy.[43–45] In a recent density functional theory study of Pd clusters, Kruger *et al.* pointed out that although free Pd nanoclusters should have a shorter bond distance than the bulk, surface oxidation can cause a strong increase in nearest-neighbor Pd–Pd bond distance associated with a significant amount of charge transfer from Pd to O.[45] Therefore, the above two observations from Fig. 4, together with the theoretical and experimental results reported in the literature, consistently imply the existence of a small number of O adsorbates on the surface of 2.7 nm Pd. Further evidence of the surface oxidation is also obtained by fitting the Pd $3d_{5/2}$ XPS spectrum of 2.7 nm Pd (not shown), which reveals a Pd–O peak. This can also satisfactorily account for the abnormal electronic behavior of the 2.7 nm MNPs observed in Figs. 3(b) and 3(c) in that the electronegative O atoms can strongly withdraw electrons from Pd atoms, resulting in a net *d*-electron depletion of the nanoparticles.

C. Simulations of the chemical adsorption effect

To further test how the oxygen adsorption will influence the XANES spectra of the MNPs, FEFF8 simulations of Pd L_3-edge XANES were conducted on various Pd cluster models, and the results are shown in Fig. 5. Figure 5(a) shows a cluster model (top) of $Pd_{55}S_{16}O_8$ together with simulated average spectra of Pd_{55}, $Pd_{55}S_8$, $Pd_{55}O_8$, $Pd_{55}S_{24}$, and $Pd_{55}S_{16}O_8$. As schematically illustrated in Fig. 5(a), O and S atoms are located on the threefold hollow sites of the Pd (111) surface. Bond distances of Pd–O and Pd–S in the cluster models are set to be 2.0 and 2.3 Å, respectively.[46,47] The $Pd_{55}O_8$ model was made by removing the 16 S from the $Pd_{55}S_{16}O_8$, and the $Pd_{55}S_{24}$ cluster was made by replacing the eight O atoms with S atoms. It should be noted that these model clusters contain only 55 Pd atoms (1.4 nm in diameter) and are smaller than a 2.7 nm Pd nanoparticle. However, a qualitative analysis of the chemical adsorption effects on the electronic properties of nanoparticles by comparing the simulated XANES of various Pd_{55} model clusters with different surface-adsorption structures should still be valid. The validity of simulations (not XANES) of the structural and electronic properties of Pd nanoparticles utilizing a 55-atom cluster has also been justified in the literature.[45]

A few important observations are noted from the simulated XANES results in Fig. 5(a). First, by comparing the spectra of Pd_{55}, $Pd_{55}S_8$, and $Pd_{55}O_8$, it is clearly seen that adsorptions of eight S and eight O atoms both cause an increase of the Pd white line intensity, indicating that *d*-charge transfers from Pd to the adsorbate atoms occur in both cases. However, the white line intensity of $Pd_{55}S_8$ is only slightly increased relative to that of Pd_{55}. In comparison, the $Pd_{55}S_8$ cluster shows a more pronounced increase in the white line intensity. This observation indicates that the amount of charge transferred to O atoms is considerably higher than that to S atoms, in agreement with the electronegativity data (Pauling electronegativity values: Pd=2.2, S=2.6, and O =3.4). In other words, the Pd–S bond is of more covalent nature, whereas the Pd–O bond is of more ionic nature. Indeed, we found that the simulated white line intensity is very sensitive to the existence of surface O atoms. Even placing four O atoms on the surface of Pd_{55} can still cause a considerable increase of the white line intensity (not shown). These results support the notion that the abnormal enhancement of the white line intensity of weakly bound 2.7 nm MNPs is associated with a small amount of surface oxide. Second, the adsorption of 24 S atoms to the Pd_{55} cluster is found to cause a sizeable increase in the white line intensity when comparing the XANES of $Pd_{55}S_{24}$ with that of Pd_{55}. In addition, the white line of $Pd_{55}S_{24}$ is found to be slightly more intense than that of $Pd_{55}O_8$. Finally, when comparing the XANES of $Pd_{55}O_8$ with that of $Pd_{55}S_{16}O_8$, it is found that further adsorption of 16 S atoms onto the surface of $Pd_{55}O_8$ (without changing the locations of eight O atoms) causes a sizeable increase in the white line intensity. This can be explained as follows: When S and O atoms coexist on the Pd surface, they both withdraw electrons from Pd atoms.

The above simulation results suggest at least theoretical evidence for asserting the existence of a small number of O adsorbates in the wet-chemically prepared weakly bound Pd MNPs. Moreover, it can also lead to a satisfactory interpretation of why there is only a very small change in the white line intensity before and after thiol capping of the 2.7 nm MNPs. After thiol substitution takes place, an important question arises concerning the fate of the O adsorbates. Generally, there could be two possibilities. The O adsorbates will either coexist with or be replaced by thiols. The trend of changes in Pd white line intensity corresponding to each possibility can be well illustrated in Fig. 5(a) by comparing the white lines of $Pd_{55}O_8$ with those of $Pd_{55}S_{16}O_8$ (coexisting model) and those of $Pd_{55}O_8$ with those of $Pd_{55}S_{24}$ (replacing model). Specifically, the simulation results in Fig. 5(a) indicate that if S and O coexist on the MNP surface (i.e., comparing $Pd_{55}O_8$ with $Pd_{55}S_{16}O_8$), there should be a sizeable increase in the white line intensity. If O adsorbates are replaced by S, the increase in white line intensity should be considerably less pronounced. This is understandable in that

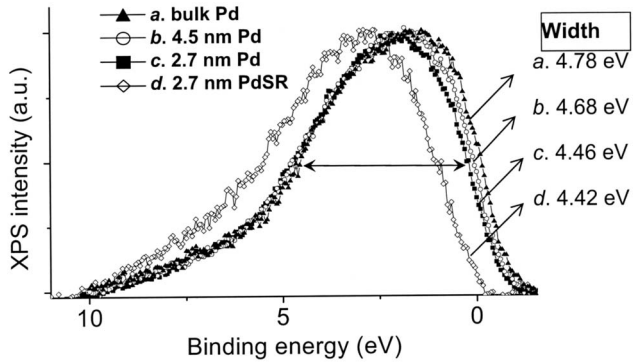

FIG. 6. XPS valence-band spectra of the three Pd MNPs and bulk Pd. The bandwidth values are given in the figure.

although the number of e-acceptors (S atoms) increases, the amount of charge each S atom gains is much smaller than that each O atom gains. If we recall the experimental observations in Figs. 2(c) and 2(d), it is immediately evident that the replacing model is in excellent agreement with the experimental data, whereas the coexisting model is not. Therefore, the abnormal change in white line intensity of the 2.7 nm MNPs, before and after the ligand substitution reaction, can be satisfactorily interpreted by taking into account two important notions. First, the weakly bound 2.7 nm MNPs have strong e-accepting O adsorbates on the particle surface. Second, these O atoms are replaced by a greater number of thiols after a ligand substitution reaction is performed. This model is consistent with the results in the literature showing that the Pd–S bonding energy is higher than the Pd–O bonding energy.[48–50] Meanwhile, thiols should also replace the weakly binding molecules (DDA and TOPB).

More simulation results are shown in Fig. 5(b), where the white line of each representative Pd site near an O adsorbate in the $Pd_{55}O_8$ cluster is compared with the identical sites in a free Pd_{55}. An illustration of the geometric position of each Pd site is also shown on top of Fig. 5(b). It can be seen that an O adsorbate only influences the white line intensity of the Pd atoms directly bound to it (site *a* and *b*). For the Pd atoms that are not directly bound to O (site *a′*, *b′*, and *c′*), the white line intensity and the fine structure remain essentially unchanged. To further prove the validity of these results, simulations using bigger Pd models (such as Pd_{309}) were also conducted, and the results are consistent. Therefore, the FEFF results indicate that the Pd–O charge transfer on the surface of a Pd cluster is very much localized, consistent with the previously published theoretical results.[51] It also points out that the electronic properties of surface Pd atoms not directly bound to O are essentially the same as those in a free Pd nanoparticle. The implications of this notion will be addressed later in the discussion of XPS data.

D. XPS studies of the size and surface effects

XPS has been known as a complementary technique to XAFS in probing the electronic properties of materials.[28] It has been particularly successful in the studies of surface and electronic properties of 2D metals and SNPs.[2,4] Figure 6 shows the valence spectra of the three MNPs and the bulk.

TABLE II. Data of XPS and XANES shifts of Pd MNPs relative to the bulk. (The uncertainty is 0.1 eV for XPS, 0.3 eV for the L_3-edge, and 0.5 eV for the L_2-edge XANES).

Sample	$3d_{5/2}$ (eV)	VB (eV)	L_3 (eV)	L_2 (eV)
4.5 nm Pd	0.20	0.15	0.0	0.0
2.7 nm Pd	0.40	0.21	0.7	0.6
2.7 nm PdSR	1.20	1.01	1.1	0.9

The values of *d*-band-width are also provided in the figure. There is a 0.1 eV *d*-band narrowing for 4.5 nm Pd relative to the bulk, whereas the two differently capped 2.7 nm MNPs both show an ~0.3 eV *d*-band narrowing. This agrees with the well documented results of *d*-band narrowing in SNPs as size decreases.[2] In addition, the *d*-band centroids of the MNPs all shift toward higher binding energies relative to the bulk. There is a 0.15 eV shift for 4.5 nm Pd, 0.21 eV for 2.7 nm Pd, and 1.01 eV for 2.7 nm PdSR. The valence shift values are also listed in Table II and will be further discussed together with the core-level data presented next.

Figure 7 shows the XPS $3d_{5/2}$ core-level spectra of the Pd samples and relevant parameters. A comparison of the core-level shift (CLS) is presented in Fig. 7(a). For the two weakly bound MNPs, it is found that the $3d_{5/2}$ peak shifts toward higher binding energies as size deceases. A positive shift of 0.20 eV relative to the bulk is found for 4.5 nm Pd and 0.40 eV for 2.7 nm Pd. For 2.7 nm PdSR, a more pronounced positive shift of 1.20 eV is found. The physical origin of the CLS of metal SNPs has been an area of considerable dispute.[2,6] Generally, two representative models have been widely used. Mason suggested that the CLS is mainly caused by initial state effects,[2] whereas Wertheim proposed that final state effects are dominant.[6] It must be noted that these two models are based on the assumption that there is virtually no charge-transfer interaction between the metals and the surrounding environment (e.g., substrate). If considerable charge transfer is involved, for instance, at the metal-substrate interface, the above two models cannot be used. Cini *et al.* proposed a different model in which the metal-substrate interfacial charge transfer is taken into account.[52] Based on studies of XPS, Auger spectroscopy, and Bremsstrahlung isochromat spectroscopy, Cini *et al.* suggested that in graphite-supported Pd SNPs, there exists considerable in-

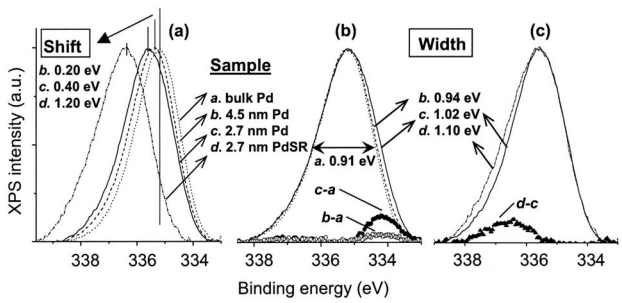

FIG. 7. XPS $3d_{5/2}$ core-level spectra of the three Pd MNPs and the bulk. (a) The original $3d$ spectra. (b) A comparison of the line shape of the two weakly bound MNPs and bulk Pd by aligning the peaks of the MNPs with that of the bulk. (c) A line shape comparison of 2.7 nm Pd and 2.7 nm PdSR by aligning the peak of 2.7 nm PdSR with that of 2.7 nm Pd.

terfacial charge transfer between the Pd 4*d* (e-donor) and the graphite π^* state (e-acceptor). This charge transfer is mainly responsible for the observed positive CLS of Pd SNPs.

The combined use of XPS and XANES in the present work provides an important opportunity to evaluate the contribution of initial state effects and final state effects to the CLS. A comparison of the edge shift of XANES and the CLS of XPS can give an assessment of the importance of the final state effects in the CLS.[52] In Table II XPS $3d_{5/2}$, valence-band and XANES $L_{3,2}$-edge data are given. It can be clearly seen that, within experimental uncertainty, Pd $3d_{5/2}$ and $L_{3,2}$-edge shifts are essentially identical. This strongly suggests that the final state effects do not play a dominant role in determining the CLS of Pd MNPs, in good agreement with the model of Cini *et al.*[52] Therefore, the model of Cini *et al.* can be used to interpret the origin of CLS of our Pd MNPs. Specifically, the CLS for MNPs mainly originates from the *d*-charge transfer from Pd atoms to the surface adsorbates, i.e., O and S. It has been known that the CLS is very sensitive to the repulsive Coulomb interaction between core and valence *d* electrons.[2] A depletion of the *d*-electron density will weaken the Coulombic repulsion, thus causing an increase in the core-level binding energy.[2] According to this model, a similar but somewhat smaller shift is expected for the shift of the centroid of the valence *d* bands because the repulsive interaction between the valence *d* electrons is less intense.[2] A comparison of the $3d_{5/2}$ CLS with the centroid shifts of valence *d* band (Table II) consistently supports this notion. The CLS values of the three MNPs are all slightly more pronounced than the valence-band shifts. However, it remains unclear why the thiol-capped MNPs exhibit a more positive shift than the weakly bound MNPs of the same size since both of them exhibit essentially the same level of *d*-electron depletion. We speculate that the number of *d*-electron deficient Pd atoms also plays a role in determining the XPS and XANES shifts. As a result, thiol-capped MNPs having a larger number of *d*-electron deficient Pd atoms will show a more positive shift than the weakly bound MNPs having a smaller number of *d*-electron deficient Pd atoms. It should also be noted that although the final state effect is not dominant, it can still contribute to some extent to the CLS values observed in Fig. 7, which might account for the slight difference between the XPS shifts and XANES shifts in Table II.

In Figs. 7(b) and 7(c), we compare the line shape of Pd samples with varied sizes (bulk, 4.5 nm Pd and 2.7 nm Pd) and capping molecules (2.7 nm Pd and 2.7 nm PdSR), respectively. In Fig. 7(b), the linewidth of the Pd $3d_{5/2}$ peak increases as the Pd size decreases. Moreover, the linewidth broadening mainly occurs at the lower binding energy side of the $3d_{5/2}$ peak. This can be more clearly seen in the difference spectra shown in Fig. 7(b). Interestingly, when comparing the line shapes of the two differently capped 2.7 nm samples, we see an opposite trend; that is, the linewidth broadening occurs at the higher binding energy side as the weakly binding molecules are replaced with thiols. The linewidth broadening observed in Fig. 7(c) can be well understood in terms of the formation of metal-sulfur bonds on the metal surface.[26,53] The Pd–S bonding causes a charge transfer from Pd to S, leaving some partial positive charge on the Pd site and thus resulting in a shoulder at the higher energy side [see the difference spectrum in Fig. 7(c)]. A similar linewidth broadening at the higher energy side has also been found in Au surfaces where charge transfer from Au to S takes place.[53] In comparison, the fact that the Pd MNPs in Fig. 7(b) do not exhibit any noticeable linewidth broadening at the higher energy side as size decreases implies that the number of O-adsorbants on the weakly bound Pd MNPs is relatively small and thus insensitive to the change in particle size. This is also consistent with the observed linewidth broadening at the lower binding energy side in Fig. 7(b). A similar linewidth broadening at the lower binding-energy side has been well documented in the 3*d* core-level XPS of a clean (or slightly O-adsorbed) 2D metal surface.[54] The negative CLS has been attributed to the lower coordination number of the surface Pd atoms than the bulk.[54] Bondzie *et al.* suggested that the negative CLS originated from the slightly enriched *d*-electron density of surface Pd atoms relative to the bulk.[37] This notion is in agreement with the model suggested by Citrin *et al.*[38] and discussed previously. It posits that the *d*-electron counts of Pd nanoparticles lie between those of bulk Pd ($d=8.22$) and isolated Pd atoms ($d=10$) and increase as the coordination number of Pd decreases. In small metal nanoparticles, there exists increasing inhomogeniety as the size decreases.[2,55] This will result in a large number of unbound surface Pd atoms with a very low coordination number (e.g., edge and corner atoms). Therefore, the linewidth broadening observed for the weakly bound MNPs can be attributed to the existence of these unbound surface atoms with very low coordination numbers.[25,26] As shown in Fig. 5(b), the electronic properties of surface Pd atoms not directly binding to O atoms are essentially the same as those in a naked Pd nanoparticle. The XPS data in Fig. 7 thus provide information consistent with the XANES data, that is, that only a small number of surface oxide is present on the weakly bound MNPs. It further points out the existence of a significant amount of unbound surface Pd atoms, with slightly increased *d*-electron counts relative to the bulk. Therefore, the XPS data, together with XAFS data and simulations, provide detailed information about the surface electronic properties of the Pd MNPs. It points out the existence of two types of surface Pd atoms in the weakly bound MNPs, i.e., oxygen-related *d*-electron deficient surface atoms and unbound surface atoms with slightly enriched *d*-electron density due to the surface inhomogeniety of MNPs. The latter has a relatively large number, whereas the former, albeit small in number, is dominant in determining the average *d*-electron counts of the MNPs due to the much higher electronegativity of O (3.4) than Pd (2.2).[45] Furthermore, the O adsorbates are replaceable with more tightly binding thiols. The thiol capping causes a considerable increase in the number of *d*-electron deficient surface Pd atoms. However, the average *d*-electron counts of Pd atoms in the MNPs before and after thiol substitution are almost unchanged due to the much lower electronegativity of S (2.6) than O (3.4).

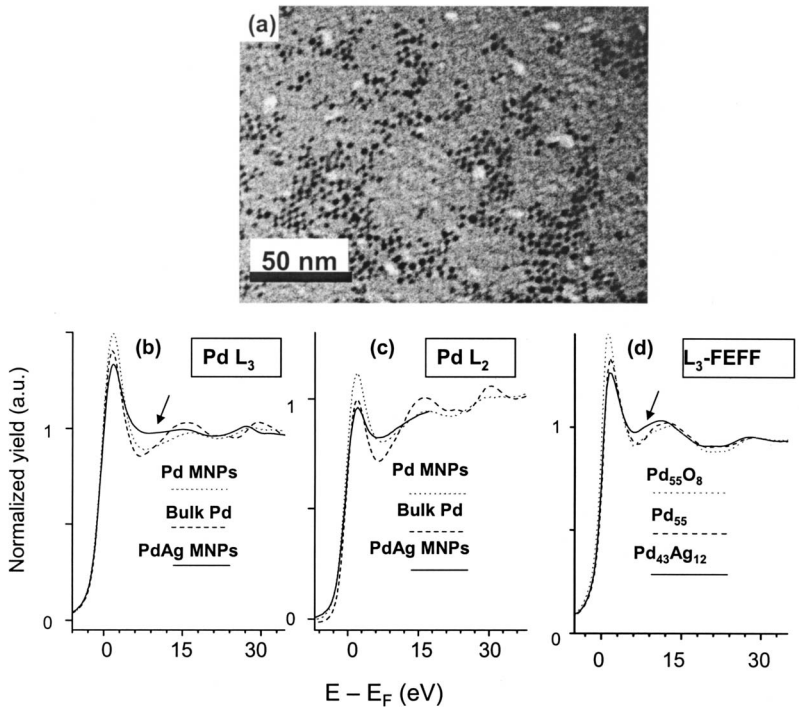

FIG. 8. (a) TEM of the 75% Pd alloy nanoparticles, (b) the Pd L_3-edge, (c) and the L_2-edge XANES of 2.7 nm Pd, bulk Pd, and 2.8 nm alloy MNPs. (d) FEFF-simulated Pd L_3-edge XANES (average spectra) of O-adsorbed Pd ($Pd_{55}O_8$), pure Pd (Pd_{55}), and PdAg alloy ($Pd_{43}Ag_{12}$). The Pd L_2-postedge structure for the Pd–Ag alloy MNPs cannot be completely collected due to the overlap with the Ag L_3-edge XANES in the higher binding energy region. The alloyed cluster was constructed with the CRYSTALMAKER program by extending a fcc unit cell consisting of 25% Ag (two face sites) and 75% Pd (eight corner sites and four face sites) to a 55-atom cluster.

E. The alloying effect

Based on the above findings, we now address the possibility of tuning the electronic behavior, specifically, the *d*-electron counts of metal MNPs.[25] The *d*-electron behavior has been found to play a critically important role in determining the catalytic properties of transition metals.[1,23,24,56] For instance, the high catalytic activities of transition metals for many reactions have been attributed to their *d*-electron deficient sites.[23] Therefore, decreasing the *d*-electron counts of the nanoparticle catalyst will lead to a higher reactivity in these reactions. On the other hand, to improve the catalytic selectivity toward some industrially important reactions, such as hydrocarbon isomerization, it is sometimes desirable to decrease the number of these *d*-electron deficient sites, that is, increase the net *d*-electron counts of the transition metal catalysts.[24] Therefore, the ability of flexibly tuning—increasingly or decreasingly—the *d*-electron counts of transition metal MNPs is of paramount importance in designing efficient catalysts with controllable reactivity and/or selectivity. From the x-ray results presented above, it is clear that surface effects, such as O chemical adsorption, which decrease the net *d*-electron counts of Pd MNPs, play a more significant role than the size effect that leads to the enrichment of *d*-electron density. As a consequence, the wet-chemically prepared Pd nanoparticles of small size seem to have inevitably decreased *d*-electron counts due to the strong influence of surface effects. The comparative studies of the weakly bound 4.5 nm Pd and 2.7 nm Pd indicate that if one desires to achieve lower *d*-electron counts in Pd, an efficient way is to simply decrease the MNP size. The smaller the MNPs, the more significant role the surface effects will play to decrease the *d*-electron counts. However, this also implies a challenge when it comes to achieving higher *d*-electron counts (i.e., gaining *d* electrons relative to the bulk) in wet-chemically prepared Pd MNPs. Indeed, it has been suggested that for metals, such as Pd and Pt, whose surfaces are catalytically reactive, surface chemical adsorption is very difficult to avoid.[57]

Here, we propose that by forming alloy MNPs of Pd with a chemically similar metal, such as Ag, such a challenge may be overcome. It has been suggested that the alloying effect is very similar to the nanosize effect in determining the electronic properties of metals; both decreasing size and diluting the metal concentration in an alloy lower than the number of like-neighbor atoms.[2] The number of like-neighbor atoms has been found to be closely correlated to the electronic properties of metals.[2,28] In the context of *d*-electron counts discussed in the present work, it is anticipated that diluting the metal concentration in an alloy consisting of Pd and a chemically similar metal will lead to an increase in the Pd *d*-electron counts.[2] This assumption is supported by the XANES experimental results for Pd–Ag bulk alloys.[28] Remarkably, the alloying effect has also been found to suppress surface chemical adsorption by weakening the metal-adsorbate interaction.[48] Therefore, the alloying effect (alloying with a chemically similar metal) can both enhance the size effect and suppress the surface effect. Toward this end, a sample of $Pd_{0.75}Ag_{0.25}$ alloy MNPs (also capped with DDA/TOPB) was synthesized using the same procedure as that for 2.7 nm Pd. The average size of the alloy MNPs revealed from TEM in Fig. 8(a) is 2.8 nm with a 12% standard deviation. Figures 8(b) and 8(c) show the Pd L_3- and L_2-edge XANESs of the Pd–Ag alloy MNPs together with those of 2.7 nm Pd and bulk Pd. It is found, as expected, that the Pd–Ag alloy MNPs exhibit a decreased white line at both edges relative to the bulk, whose white lines are still less intense than those of 2.7 nm Pd. This indicates that the 2.8 nm alloy MNPs have increased *d*-electron counts relative to bulk Pd, whereas the 2.7 nm Pd, due to the surface adsorption by oxygen, have decreased *d*-electron counts. In

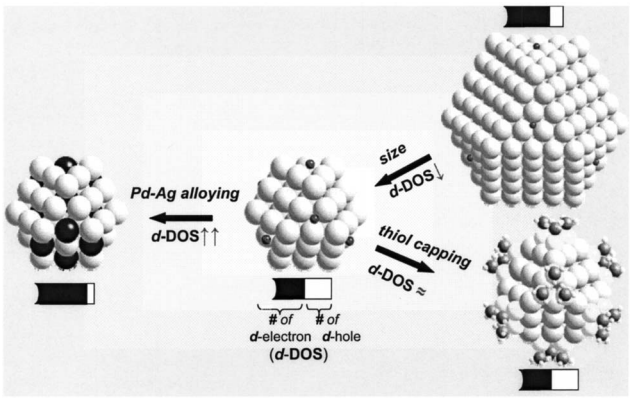

SCHEME 1. A schematic illustration of the size, surface, and alloying effects on the *d*-electron counts (denoted as *d*-DOS in the scheme) of Pd nanoparticles. The capping molecules of the weakly bound MNPs are not shown. For simplification purposes, the $-SCH_3$ groups are used to represent the dedecanethiol capping molecules in the strongly bound MNPs.

Fig. 8(d), FEFF8 simulated Pd L_3-edge XANES is presented, taking into account the surface effect (O-adsorption) and alloying effects on the Pd L_3-edge white line intensities. It is evident from the simulations that the alloying effect results in a decrease of the white line intensity, whereas the O-adsorption effect causes an increase. Evidence of the existence of Pd–Ag alloying interaction in the 2.8 nm Pd–Ag sample is also found from the identical spectral features marked by arrows in Figs. 8(b) and 8(d). Therefore, the results from Fig. 8, together with other results previously presented, illustrate that by properly manipulating the surface, size, and alloying effects, the tunable electronic behavior of Pd nanoparticles can be achieved. It is also implied that the surface chemical structure of Pd nanoparticles may be tailored by controlling the above three effects. A summary of these mechanisms is schematically presented in Scheme 1.

IV. CONCLUSION

In summary, we have used the ligand substitution reaction, Pd $L_{3,2,1}$-edge and S *K*-edge XAFSs, XAFS simulations, and valence-band and core-level XPS to systematically investigate the surface structural and electronic properties of wet-chemically prepared Pd nanoparticles of varied size, molecular capping, and metal composition. There are three significant findings from this work. First, the surface chemical characteristics of Pd MNPs before and after the ligand substitution are interpreted at the atomic level. Second, the surface electronic properties of Pd MNPs are presented in detail, including the existence of Pd atoms enriched by *d* electrons due to the surface inhomogeniety and Pd atoms deficient in *d* electrons induced by O adsorption in weakly bound MNPs. It is also revealed that there exist a large number of *d*-electron deficient surface Pd atoms caused by Pd–S bonding in the thiol-capped Pd MNPs. The relative significance of each type of surface Pd atoms in determining the net *d*-electron counts of the MNPs are also identified. Finally, this work illustrates that by properly manipulating the surface, size, and alloying effects, Pd-based MNPs with tunable electronic behavior can be achieved. It is also implied that the surface chemical structure of Pd nanoparticles may be tailored by controlling the above three effects. It is anticipated that the strategy of tuning the electronic properties and tailoring the surface structures of Pd MNPs presented here should also be applicable to other catalytically active metals, such as Pt and Rh, and will find applications in designing efficient nanoparticle catalysts with controllable reactivity and/or selectivity.[1,23,24] Moreover, the detailed picture of the surface structural and electronic properties of Pd MNPs revealed in this work will add useful information to a number of fundamentally important areas, such as the catalytic mechanism of Pd nanoparticles,[23] the sulfur-poisoning mechanism of Pd catalysts,[56] and the unusual magnetic behavior of Pd MNPs.[58–60]

ACKNOWLEDGMENTS

This research is financially supported by Dalhousie University and NSERC Canada. The authors also acknowledge financial support from the Killam Trusts, the Canada Foundation for Innovation, the Atlantic Innovation Fund, and other partners that fund the Facilities for Characterization of Materials managed by the Institute for Research of Materials (IRM). The synchrotron facility at SRC is funded by U.S. NSF under Award No. DMR-0537588, and the CSRF DCM beamline is supported by NSERC Canada. We acknowledge the CSRF staff and Dr. Astrid Jurgensen for the synchrotron technical support and the IRM staff and Dr. Zeynel Bayindir for the XPS measurements.

[1] M. G. Mason, L. J. Gerenser, and S. T. Lee, Phys. Rev. Lett. **39**, 288 (1977).
[2] M. G. Mason, Phys. Rev. B **27**, 748 (1983).
[3] G. K. Wertheim, S. B. Dicenzo, and S. E. Youngquist, Phys. Rev. Lett. **51**, 2310 (1983).
[4] P. H. Citrin and G. K. Wertheim, Phys. Rev. B **27**, 3176 (1983).
[5] G. K. Wertheim, S. B. Dicenzo, and D. N. E. Buchanan, Phys. Rev. B **33**, 5384 (1986).
[6] G. K. Wertheim, Z. Phys. D: At., Mol. Clusters **12**, 319 (1989).
[7] R. P. Andres, J. D. Bielefeld, J. I. Henderson, D. B. Janes, V. R. Kolagunta, C. P. Kubiak, W. J. Mahoney, and R. G. Osifchin, Science **273**, 1690 (1996).
[8] D. Bazin, D. Sayers, J. J. Rehr, and C. Mottet, J. Phys. Chem. B **101**, 5332 (1997).
[9] S. H. Joo, S. J. Choi, I. Oh, J. Kwak, Z. Liu, O. Terasaki, and R. Ryoo, Nature (London) **412**, 169 (2001).
[10] G. A. Somorjai, R. L. York, D. Butcher, and J. Y. Park, Phys. Chem. Chem. Phys. **9**, 3500 (2007).
[11] M. Baumer and H. J. Freund, Prog. Surf. Sci. **61**, 127 (1999).
[12] M. Haruta and M. Date, Appl. Catal., A **222**, 427 (2001).
[13] M. Brust, M. Walker, D. Bethell, D. J. Schiffrin, and R. Whyman, J. Chem. Soc., Chem. Commun. **1994**, 801 (1994).
[14] G. Schmid and L. F. Chi, Adv. Mater. (Weinheim, Ger.) **10**, 515 (1998).
[15] A. C. Templeton, M. P. Wuelfing, and R. W. Murray, Acc. Chem. Res. **33**, 27 (2000).
[16] R. M. Crooks, M. Q. Zhao, L. Sun, V. Chechik, and L. K. Yeung, Acc. Chem. Res. **34**, 181 (2001).
[17] M. C. Daniel and D. Astruc, Chem. Rev. (Washington, D.C.) **104**, 293 (2004).
[18] C. J. Murphy, T. K. San, A. M. Gole, C. J. Orendorff, J. X. Gao, L. Gou, S. E. Hunyadi, and T. Li, J. Phys. Chem. B **109**, 13857 (2005).
[19] J. A. Dahl, B. L. S. Maddux, and J. E. Hutchison, Chem. Rev. (Washington, D.C.) **107**, 2228 (2007).
[20] M. Bruchez, M. Moronne, P. Gin, S. Weiss, and A. P. Alivisatos, Science **281**, 2013 (1998).
[21] F. Caruso, Adv. Mater. (Weinheim, Ger.) **13**, 11 (2001).
[22] M. Tamura and H. Fujihara, J. Am. Chem. Soc. **125**, 15742 (2003).
[23] J. H. Sinfelt and G. D. Meitzner, Acc. Chem. Res. **26**, 1 (1993).

[24] G. A. Somorjai, *Introduction to Surface Chemistry and Catalysis* (Wiley, New York, 1994).
[25] P. Zhang and T. K. Sham, Appl. Phys. Lett. **81**, 736 (2002).
[26] P. Zhang and T. K. Sham, Phys. Rev. Lett. **90**, 245502 (2003).
[27] A. E. Saunders, M. B. Sigman, and B. A. Korgel, J. Phys. Chem. B **108**, 193 (2004).
[28] I. Coulthard and T. K. Sham, Phys. Rev. Lett. **77**, 4824 (1996).
[29] A. L. Ankudinov, B. Ravel, J. J. Rehr, and S. D. Conradson, Phys. Rev. B **58**, 7565 (1998).
[30] A. L. Ankudinov, J. J. Rehr, J. J. Low, and S. R. Bare, J. Chem. Phys. **116**, 1911 (2002).
[31] P. Zhang and T. K. Sham, Appl. Phys. Lett. **82**, 1778 (2003).
[32] P. Zhang, P. S. Kim, and T. K. Sham, Appl. Phys. Lett. **82**, 1470 (2003).
[33] M. De Crescenzi, E. Colavita, U. Del Pennino, P. Sassaroli, S. Valeri, C. Rinaldi, L. Sorba, and S. Nannarone, Phys. Rev. B **32**, 612 (1985).
[34] T. K. Sham, Phys. Rev. B **31**, 1888 (1985).
[35] T. K. Sham, Phys. Rev. B **31**, 1903 (1985).
[36] I. Coulthard, S. Degen, Y. J. Zhu, and T. K. Sham, Can. J. Chem. **76**, 1707 (1998).
[37] V. A. Bondzie, P. Kleban, and D. J. Dwyer, Surf. Sci. **347**, 319 (1996).
[38] P. H. Citrin, G. K. Wertheim, and Y. Baer, Phys. Rev. Lett. **41**, 1425 (1978).
[39] M. Gothelid, H. von Schenck, J. Weissenrieder, B. Akermark, A. Tkatchenko, and M. Galvan, Surf. Sci. **600**, 3093 (2006).
[40] J. D. Grunwaldt, M. Caravati, and A. Baiker, J. Phys. Chem. B **110**, 25586 (2006).
[41] J. D. Grunwaldt, M. Caravati, and A. Baiker, J. Phys. Chem. B **110**, 9916 (2006).
[42] M. De Crescenzi, M. Diociaiuti, P. Picozzi, and S. Santucci, Phys. Rev. B **34**, 4334 (1986).
[43] R. Lamber, S. Wetjen, and N. I. Jaeger, Phys. Rev. B **51**, 10968 (1995).
[44] E. Z. daSilva and A. Antonelli, Phys. Rev. B **54**, 17057 (1996).
[45] S. Kruger, S. Vent, F. Nortemann, M. Staufer, and N. Rosch, J. Chem. Phys. **115**, 2082 (2001).
[46] H. Murayama, N. Ichikuni, Y. Negishi, T. Nagata, and T. Tsukuda, Chem. Phys. Lett. **376**, 26 (2003).
[47] F. P. Leisenberger, G. Koller, M. Sock, S. Surnev, M. G. Ramsey, F. P. Netzer, B. Klotzer, and K. Hayek, Surf. Sci. **445**, 380 (2000).
[48] D. R. Alfonso, A. V. Cugini, and D. S. Sholl, Surf. Sci. **546**, 12 (2003).
[49] K. Honkala and K. Laasonen, J. Chem. Phys. **115**, 2297 (2001).
[50] J. Roques, C. Lacaze-Dufaure, and C. Mijoule, J. Chem. Theory Comput. **3**, 878 (2007).
[51] H. Sellers, Chem. Phys. Lett. **170**, 5 (1990).
[52] M. Cini, M. De Crescenzi, F. Patella, N. Motta, M. Sastry, F. Rochet, R. Pasquali, A. Balzarotti, and C. Verdozzi, Phys. Rev. B **41**, 5685 (1990).
[53] T. K. Sham, P. S. G. Kim, and P. Zhang, Solid State Commun. **138**, 553 (2006).
[54] J. N. Andersen, D. Hennig, E. Lundgren, M. Methfessel, R. Nyholm, and M. Scheffler, Phys. Rev. B **50**, 17525 (1994).
[55] S. B. Dicenzo, S. D. Berry, and E. H. Hartford, Phys. Rev. B **38**, 8465 (1988).
[56] J. A. Rodriguez and J. Hrbek, Acc. Chem. Res. **32**, 719 (1999).
[57] C. Kuhrt and R. Anton, Thin Solid Films **198**, 301 (1991).
[58] B. Sampedro, P. Crespo, A. Hernando, R. Litran, J. C. S. Lopez, C. L. Cartes, A. Fernandez, J. Ramirez, J. G. Calbet, and M. Vallet, Phys. Rev. Lett. **91**, 237203 (2003).
[59] A. Hernando, P. Crespo, M. A. Garcia, E. F. Pinel, J. de la Venta, A. Fernandez, and S. Penades, Phys. Rev. B **74**, 052403 (2006).
[60] R. Litran, B. Sampedro, T. C. Rojas, M. Multigner, J. C. Sanchez-Lopez, P. Crespo, C. Lopez-Cartes, M. A. Garcia, A. Hernando, and A. Fernandez, Phys. Rev. B **73**, 054404 (2006).